ISSN 1674-1056
http://cpb.iphy.ac.cn
http://iopscience.iop.org/cpb
中国物理 B
Chinese Physics
中国物理
Chinese Physics B

Electro-optical properties and (*E*, *T*) phase diagram of fluorinated chiral smectic liquid crystals

R Zgueb, H Dhaouadi, T Othman

Citation: Chin. Phys. B . 2018, 27(10): 107701. **doi:** 10.1088/1674-1056/27/10/107701

Journal homepage: http://cpb.iphy.ac.cn; http://iopscience.iop.org/cpb

What follows is a list of articles you may be interested in

Crystallization behaviors of ultrathin Al-doped HfO_2 amorphous films grown by atomic layer deposition

Xue-Li Ma(马雪丽), Hong Yang(杨红), Jin-Juan Xiang(项金娟), Xiao-Lei Wang(王晓磊), Wen-Wu Wang(王文武), Jian-Qi Zhang(张建齐), Hua-Xiang Yin(殷华湘), Hui-Long Zhu(朱慧珑), Chao Zhao(赵超)

Chin. Phys. B . 2017, 26(2): 027701. **doi:** 10.1088/1674-1056/26/2/027701

Field-induced phase transitions in chiral smectic liquid crystals studied by the constant current method

H Dhaouadi, R Zgueb, O Riahi, F Trabelsi, T Othman

Chin. Phys. B . 2016, 25(5): 057704. **doi:** 10.1088/1674-1056/25/5/057704

Electric properties and phase transition behavior in lead lanthanum zirconate stannate titanate ceramics with low zirconate content

Zeng Tao, Lou Qi-Wei, Chen Xue-Feng, Zhang Hong-Ling, Dong Xian-Lin, Wang Gen-Shui

Chin. Phys. B . 2015, 24(11): 117702. **doi:** 10.1088/1674-1056/24/11/117702

Dielectric and ferroelectric properties of $Sr_4CaSmTi_3Nb_7O_{30}$ with tetragonal tungsten bronze structure

Gong Gao-Shang, Fang Yu-Jiao, Huang Shuai, Yin Chong-Yang, Yuan Song-Liu, Wang Li-Guang

Chin. Phys. B . 2014, 23(9): 097701. **doi:** 10.1088/1674-1056/23/9/097701

Dielectric spectroscopy studies of ZnO single crystal

Cheng Peng-Fei, Li Sheng-Tao, Wang Hui

Chin. Phys. B . 2013, 22(10): 107701. **doi:** 10.1088/1674-1056/22/10/107701

Electro-optical properties and (E,T) phase diagram of fluorinated chiral smectic liquid crystals

R Zgueb[†], H Dhaouadi, and T Othman

Université Tunis El-Manar, Faculté des Sciences de Tunis, Laboratoire de physique de la matière molle et de modélisation électromagnétique (LP3ME), Campus Universitaire Farhat Hached 2092 *Tunis Tunisie*

(Received 3 April 2018; revised manuscript received 25 July 2018; published online 27 September 2018)

Fluorinated smectic liquid crystals each with a biphenyl benzoate rigid core are investigated. Molecular structures of the studied compounds have difference only in fluorine position and the length of the carbon chain. Dielectric relaxation study and electro-optical measurements are carried out with the classical *SSFLC* geometry. The field-induced phase transitions are studied and the (E,T) phase diagram is established.

Keywords: smectic liquid crystal, dielectric relaxation, electro–optical properties, phase transition, (E,T) phase diagram

PACS: 77.84.–s, 77.80.–e, 64.70.M–, 64.70.mj **DOI:** 10.1088/1674-1056/27/10/107701

1. Introduction

Liquid crystals play an already important and still growing role in a variety of displays, modulators and a host of other electro–optical devices. Ferroelectric liquid crystals are promising materials for fast switching electro-optical displays with wide viewing angle.[1] Incorporating chiral smectic liquid crystals into display devices is extremely attractive.[2,3] But their widespread commercial use has not yet been realized. An active research revolves around the synthesis of new chiral smectic compound that possesses specific physical properties. In practice, very few elements can be used to modify the structure and properties of mesogenic phases, and thus retaining the mesogenity. Among substituents, the fluorine is very important one. Furthermore, the small size and high polarity of a fluoro-substituent can have some remarkable effects on the physical properties of liquid crystals. Phase behaviors,[4,5] physical,[6,7,11] dielectric,[12,13] and electro–optical[4,9,11–15] properties of fluorinated derivatives are dependent on the lateral fluoro-substituent location.[6–10] Such a variety leads to the interesting and advantageous tailoring of properties, both for establishing structure–property relationships, and for creating new applications.[2,3,11]

In smectic liquid crystals the molecules are arranged in layers with the director tilted with respect to the layer normal by a temperature-dependent tilt angle. Many phases are encountered with the same tilt inside the layers but a distribution of the azimuthal direction which is periodic with a unit cell of one (SmC^*), two (SmC^*_A), three (SmC^*_{Fi1}), four (SmC^*_{Fi2}) or more (SmC^*_α) layers. In most of these phases, the layer normal is a symmetry axis so there is no macroscopic polarization except for the SmC^* and SmC^*_{Fi1} which are polar phases.

By the application of a sufficiently high electric field, in all these phases usually occurs a transition to the unwound SmC^*_{unwound} phase, where the helical structure is totally destructed. Hireoka *et al.* detected an unwinding of helix followed by a field-induced transition from the ferrielectric three-layer phase to the SmC^*_{unwound} phase.[16] This result is obtained from the apparent angle measurements according to applied electric field. Indeed, Hireoka *et al.* performed the angle measurement and conoscopic observations at various temperatures.

Isozaki *et al.* reported a field-induced phase transitions from a 3-layer intermediate phase to the SmC^*_{unwound} phase in the binary mixtures of MHPOCBC and MHPOOCBC.[17] Marcerou *et al.* traced the first experimental field–temperature phase diagram of a fluorinated chiral smectic compound.[18] Research focusing on the study of field-induced phase transitions is useful in applications of display device because of the importance of knowing the phase stability.[18–21]

In this paper, we first focus on the influence of the chemical structure on the diversity of the phases present for certain liquid crystals. Second, we report the main results concerning the influence of the fluorine position on the electro-optical properties and the (E,T) phase diagrams of two chiral smectic compounds.

2. Theoretical background

In this section we present the results of thermodynamic studies of the phases transitions in chiral smectic liquid crystals. The classical thermodynamic approach makes it possible to explain the (E,T) phase diagram while the Landau–Degenne development makes it possible to envisage the evolution of the dielectric permittivity according to the temperature and thus to explain the experimental results of dielectric

[†]Corresponding author. E-mail: rihab_zgueb@yahoo.fr

© 2018 Chinese Physical Society and IOP Publishing Ltd

spectroscopy.

For the study of ferroelectric liquid crystals one must consider in addition to the common thermodynamic parameters the pressure p, the volume V, the temperature T, and the entropy S, two other electric parameters: the electric field E and the electric excitation D. Consequently, the variance of the system, " ferroelectric liquid crystal confined in an SSFLC cell", becomes

$$v = C + 3 - \varphi, \tag{1}$$

where C is the number of components (equation (1) is for a pure substance) and φ is the number of phases, number 3 indicates the three intensive variables of the system: pressure p, temperature T, and electric field E.

For a pure substance the variance when two phases coexist is 2. The experiments on the liquid crystals are generally carried out at constant pressure, so that during a transition under electric field at constant temperature the value of the electric field is thermodynamically imposed.[22] If the transition is of the first order, the equilibrium between two phases results in a constant value of the electric field. We will therefore have $\delta E = 0$ along the transition.

In the mean-field theory of the para-ferroeletric transition, if we consider the polarization P as an order parameter the Landau free energy is given as follows:[23]

$$g = g_0 + \frac{1}{2}\alpha(T - T_c)P^2 + \frac{1}{4}bP^4. \tag{2}$$

The polarization of the system is zero above T_c, elsewhere it is equal to

$$P = \sqrt{\frac{\alpha}{b}(T - T_c)}. \tag{3}$$

In thermodynamics the quadratic term of this development can be written as

$$\frac{1}{2}\alpha(T - T_c)P^2 = \frac{1}{2\varepsilon_0\chi}P^2. \tag{4}$$

With an applied electric field (E), the energy with considering only the quadratic term becomes

$$g = g_0 + \frac{1}{2}\alpha(T - T_c)P^2 - \frac{1}{2}\varepsilon_0\varepsilon E^2 - PE. \tag{5}$$

Minimizing P, the effective value of ferroelectric polarization P_{ferro} is obtained as follows:

$$P_{\text{ferro}} = \varepsilon_0\chi E = \frac{1}{\alpha(T - T_c)}E. \tag{6}$$

The total polarization of the sample can be written as

$$E = \varepsilon_0\chi_\alpha E + P_{\text{ferro}}. \tag{7}$$

Then the following equation is obtained

$$\varepsilon = 1 + \chi_\infty + \frac{1}{\varepsilon_0\alpha(T - T_c)}, \tag{8}$$

where χ_∞ is the dielectric susceptibility which involves mainly electronic contributions.

The phase transition can be lolated either by measuring the polarization P which vanishes at T_c or by looking for the dielectric constant ε and its divergence at T_c.

Now, if we consider the tilt angle as the principle order parameter, Landau's free energy is then written as

$$g = g_0 + \frac{1}{2}\alpha(T - T_c)\theta^2 + \frac{1}{4}B\theta^4 + \frac{1}{2\varepsilon_0\chi_\perp}P^2 - CP\theta. \tag{9}$$

Minimizing P, one obtains a polarization proportional to the tilt angle θ as given by

$$P = \varepsilon_0\chi_\perp C\theta. \tag{10}$$

With an applied electric field parallel to the smectic layers, the dielectric susceptibility diverges also in the vicinity of the effective transition temperature T_c^* due to the linear coupling between the polarization and the tilt angle. We spoke about the electro-clinic effect.

$$g = g_0 + \frac{1}{2}\alpha(T - T_c)\theta^2 + \frac{1}{2\varepsilon_0\chi_\perp}P^2 - CP\theta - \frac{1}{2}\varepsilon_0\varepsilon E^2 - PE. \tag{11}$$

For a sinusoidal electric field of pulsation ω, the polarization above T_c^* is

$$P = \varepsilon_0\chi_\perp E\left(1 + \frac{\varepsilon_0\chi_\perp C^2}{\alpha(T - T_c^*) + j\gamma\omega}\right) = \varepsilon_0\tilde{\chi}_\perp E. \tag{12}$$

There is then a contribution to $\varepsilon_\perp$ which diverges at T_c^* where the relaxation frequency vanishes; it is the electro-clinic soft mode.[24]

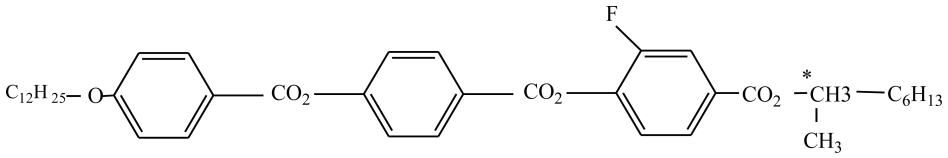
3. Experiment

The liquid crystals studied are chiral smectic compounds belonging to two series of fluorinated products C_nF_3 and C_nF_2 ($n = 7$, 8, 10, and 12).[25,26] The molecular structure of these compounds and the zero-field phase sequence defined by dielectric spectroscopy are shown in Fig. 1.

The smectic chiral compounds mentioned above were investigated by means of polarizing microscopy between crossed polarizers, where we used a polyimide coated planer glass cell with indium tin oxide (ITO) electrodes of 5-μm cell thickness.

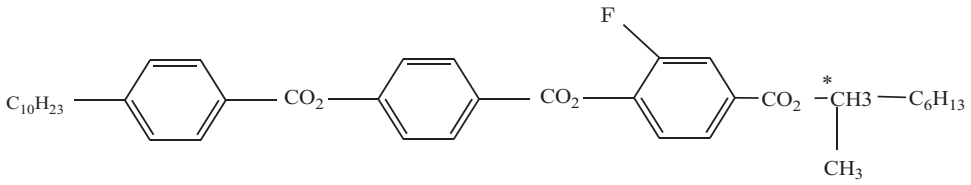
We carried out experiments on the two products $C_{12}F_3$ and C_8F_2. The found results are compared with those of the products $C_{10}F_3$ and C_7F_2 in order to highlight the effects of the fluorine position and length of the carbonaceous chains on the properties of these products.

(i) Compound $C_{12}F_3$



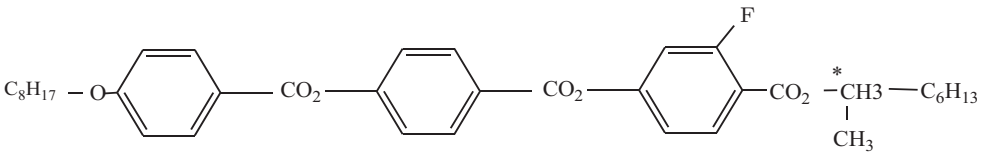
1(a). *Cr* (60 °C) – $SmC^*_{Fi_2}$ (67.2 °C) – $SmC^*_{Fi_1}$ + SmC^* (79.4 °C) – SmC^* (88 °C) – SmC^*_α (88.6 °C) – SmA^* (106 °C) – *I*.

(ii) Compound $C_{10}F_3$



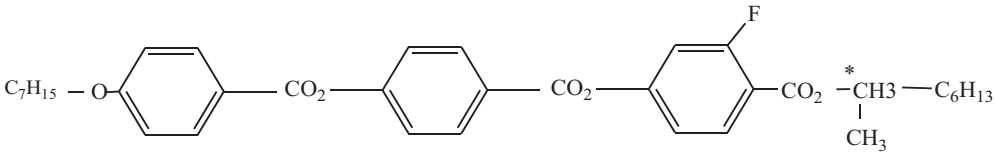
1(b). $SmC^*_{Fi_2}$ (64 °C) – SmC^*_α (73.6 °C) – SmA^* (108 °C) – *I*.

(iii) Compound C_8F_2



1(c). $SmCA^*$ (107.6 °C) – $SmC^*_{Fi_1}$ (109.4 °C) – SmC^*_α (110.8 °C) – SmA^* (140.7 °C) – *I*.

(iv) Compound C_7F_2



1(d). SmC^*_A (103.5 °C) – SmC^*_α (107.3 °C) – SmA^* (144.5 °C) – *I*.

Fig.1. Chemical structures and the phase sequences of $C_{12}F_3$, $C_{10}F_3$, C_8F_2, and C_7F_2 compounds.

In the dielectric and electro-optic measurements, 5-μm commercial cells (EHC, Japan), with 25-mm^2 ITO electrodes coated by polyimide, were used. The cells were filled in the isotropic phase. Textures of experimental cells were observed by using a polarizing microscope. Applying the electric field to the sample cell was provided by the voltage generator (Tektronix AWG 2021) delivering a static voltage up to 5 V, connected to an amplifier (Krohn–Hite Model 7500 Amplifier). The electro–optic measurements were performed with the electro–optic response from the sample placed between crossed polarizers.

Dielectric spectroscopy studies were performed with a 7280 DSC lock-in amplifier that allowed measurements in the frequency window 10 Hz–2 MHz. During measurements, this system enabled us to superimpose direct bias voltages. The dielectric dispersion data were analyzed by fitting the temperature-dependent complex dielectric constant to the Cole–Cole equation:

$$\varepsilon^*(\omega) - \varepsilon_\infty = \sum_k \frac{\Delta\varepsilon_k}{1 + (\mathrm{i}\omega\tau_k)^{1-\alpha_k}},$$

where ε_∞ is the high frequency permittivity, $\Delta\varepsilon_k$, τ_k, and α_k are the dielectric relaxation strengths, relaxation times, and the distribution parameters ($0 < \alpha_k < 1$), respectively, for the k-th relaxation process. For a single Debye-type relaxation, the distribution parameter is equal to zero.

4. Result and discussion

4.1. Dielectric spectroscopy

Figure 2 shows the plot of the dielectric absorption spectrum as a function of frequency and temperature for the compound C_8F_2.

The peak at 110.8 °C is due to the soft mode (field-induced fluctuations in θ, also called electro–clinic effect) and indicates the low temperature border of SmA^*. At lower temperatures, a low frequency mode is observed at 109.4 °C. This

mode is due to some azimuthal reorientation of the molecules, and the absorption can be attributed to Goldstone ferrielectric mode (Fig. 3). Therefore, this mode clearly shows that here is the ferrielectric polar phase $SmC^*_{Fi_1}$. For a lower temperature of 107.9 °C, Figure 2 shows a very low dielectric absorption ε'' value and relatively high relaxation frequency which characterizes the soft mode corresponding to the antiferroelectric phase SmC^*_A.

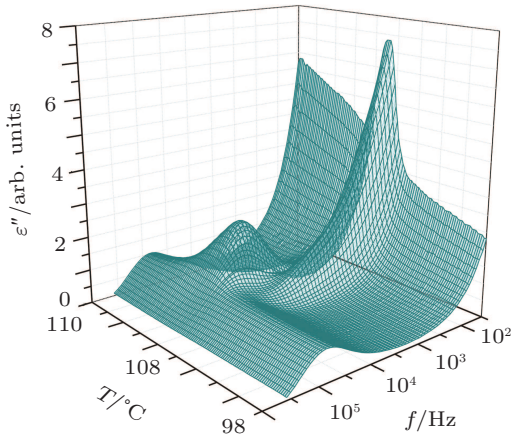


Fig. 2. (color online) Three-dimensional plot of the imaginary part ε'' of dielectric permittivity versus frequency (10 Hz–2 MHz) and temperature (98 °C–119 °C). The cell thickness is 5 μm.

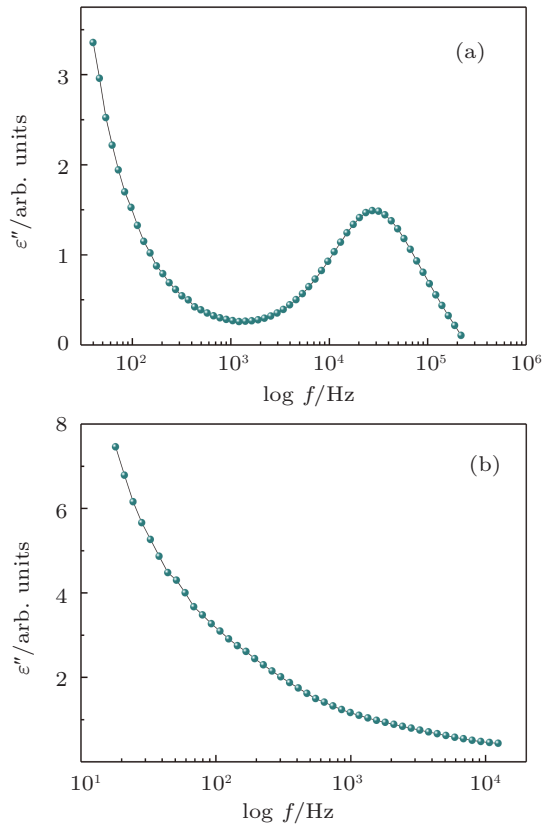


Fig. 3. (color online) Dependence of ε'' on frequency for (a) SmC^*_α and (b) $SmC^*_{Fi_1}$.

We have already reported the phase sequence of $C_{12}F_3$ compound and we detect the coexistence of the two polar phases, SmC^* and $SmC^*_{Fi_1}$ in a wide temperature range from 79.4 °C to 67.6 (Fig. 4).[27]

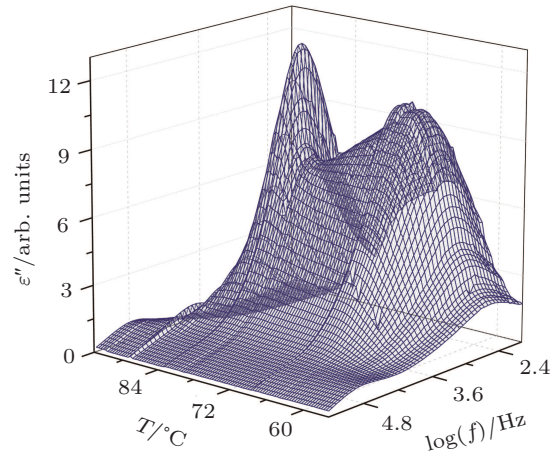


Fig. 4. (color online) Three-dimensional plot of the imaginary part ε'' of dielectric permittivity versus frequency (100 kHz–300 kHz) and temperature (95 °C–55 °C) for $C_{12}F_3$ compound with cell thickness 5 μm.

Molecular structures of the compounds $C_{12}F_3$ and $C_{10}F_3$ differ only by the length of the carbon chain. The clarification temperatures decrease with the alkyl chain length increasing. In addition, they are lower for these compounds than C_8F_2 and C_7F_2.

The alkyl chain length also affects the mesomorphic behavior. Indeed, when the molecular length decreases, the domain of existence of the SmA^* phase diminishes which is of benefit to the domain of existence of tilted smectic phases. Furthermore, the existence range of SmA^* phase in C_8F_2 compound is less than that of C_7F_2, the same report is also to be made in the case of the $C_{12}F_3$ and $C_{10}F_3$ compounds.

We note that the re-positioning of the fluorine atom from the 2- to the 3-position of the first benzene ring with respect to the chiral chain induces a transition mesophases temperature to decrease. Further, the fluorine position affects heavily the presence of certain phases. The temperature range of existence for the SmA^* phase is almost half in the $C_{12}F_3$ compound compared within the C8F2 compound. The SmC^*_α phase is stabilized in the short chains (C_7F_2 and $C_{10}F_3$). The SmC^*_A phase is absent in compounds with fluorine position 3. We note that the SmC^*_A phase is strongly stabilized in the C_8F_2 compound, while absent in the $C_{12}F_3$ or $C_{10}F_3$ compound.

Concerning the appearance of polar phases, things are more ambiguous. The polar phases are missing in the compounds $C_{10}F_3$ and C_7F_2. The compound C_8F_2 present only the ferrielectric $SmC^*_{Fi_1}$ phase in a very small temperature range, only 1.8 °C, whereas this phase is coexistent with the ferroelectric SmC^* one at a wide temperature range (12.2 °C) for the $C_{12}F_3$ compound.

4.2. Optimized geometry by using molecular mechanics

To explicate the structure property, the relationship geometries of the molecules are optimized by using the PM3 molecular mechanics method in a Chem–Draw–Ultra package.[28] The optimized structures of the molecules are

shown in Fig. 5. The optimized lengths of the molecules are 34.9, 36.05, 38.37, and 41.09 Å for C_7F_2, C_8F_2, $C_{10}F_3$, and $C_{12}F_3$ respectively, showing quite strong dipole moments for all these compounds.

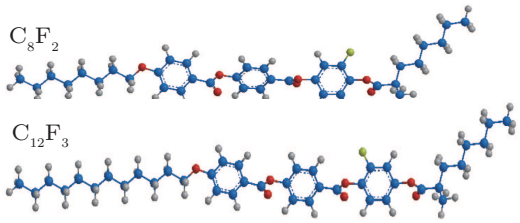


Fig. 5. (color online) Optimized geometry of (a) C_8F_2 and (b) $C_{12}F_3$.

The dipole moment is 3.3 D for the liquid crystals $C_{10}F_3$ and $C_{12}F_3$. Those of the compounds C_8F_2 and C_7F_2 have closed values 4.63 D and 4.62 D, respectively. Then it is the position of the fluorine atom, located on the benzene near the chiral center that affects the dipole moment but not the chain length. The value of the dipole moment increases for the compound with fluorine in the 2-position in benzene. The molecules structures are optimized with 0.09-kcal/Å molgradient. The dipole moment for C_8F_2 holds the value 4.63 D with the components −3.76, −1.4, and 2.3 D; then for $C_{12}F_3$ is equal to 3.3 D with components −2.1, −1.13, and 2.39 D. It is observed that the dipole moment increases systematically as fluorine atom moves from 3 to 2-position in benzene near chiral center as expected.

On the other hand, by comparing the molecular structures of C_nF_3 and C_nF_2 compounds, one notice a decrease in the distance between the fluorine atom and the chiral centre from 6.9 Å to 4.48 Å. The dipole moment is observed to increase. This rise in the dipolar moment is caused by the increased coupling between the dipole at the chiral center and the lateral molecular dipole. This is because of the electro-accepting fluorine substitution and the induction of the electric charge close to the dipole moment of the carbonyl group located close to the chiral center. This clearly illustrates that the electronic effects of a lateral fluoro-substituent are strongly dependent on the location.

4.3. Electro–optical properties

To study the spontaneous polarization P_s and the tilt angle θ, we use the surface stabilized ferroelectric liquid crystal configuration (SSFLC). The sample thickness is about 5 μm. The spontaneous polarization measurements use the same experimental set-up as the tilt angle measurements, with the amplitude of the electric field necessary to saturate the polarization being around 5 $V \cdot \mu m^{-1}$ and the frequency about 40 Hz. The reversal of the electric field reverses the polarization. The electric charge carried gives rise to the macroscopic polarization. In order to measure the temperature variation of the tilt angle, a low frequency and high amplitude electric field ($E = 5\ V \cdot \mu m^{-1}$; $f = 0.2$ Hz) is applied to the samples. The value of tilt angle is measured by using the usual 2θ optical method.[29] The tilt angle measurements use the same experimental set-up as the spontaneous polarization measurements.

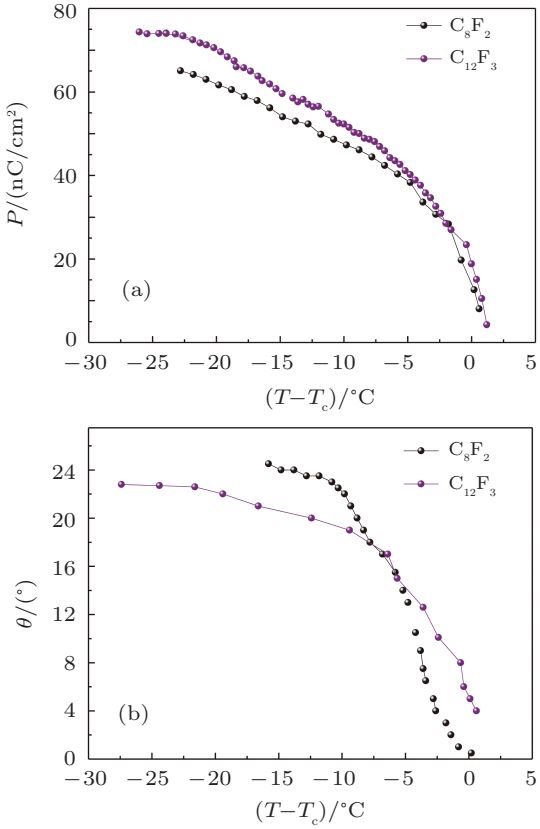


Fig. 6. (color online) Dependence of (a) spontaneous polarization P_s and (b) tilt angle θ on reduced temperature ($T - T_c$), where T_c is the SmA^*–SmC^*_α transition temperature.

Figures 6(a) and 6(b) show the temperature dependence of the spontaneous polarization P_s and tilt angle θ of the C_8F_2 and $C_{12}F_3$ compounds. As expected, the material presents a gradually changing polarization and tilt. Starting from low values the polarization approaches to the SmA^*–SmC^*_α transition and continuously increases with temperature decreasing progressively. The values of the saturated polarizations are not very high, similar to those for many three-ring compounds. The saturated values are around 80 nC/cm^2 and 70 nC/cm^2 for $C_{12}F_3$ and C_8F_2 respectively. The tilt angle decreases as the temperature approaches to the SmA^*–SmC^*_α transition temperature, like that polarization behavior. Its maximum value was about 23° and 25° for $C_{12}F_3$ and C_8F_2. For C_8F_2, tilt angle is found to increase quickly at 110.8 °C in the 3-layer $SmC^*_{Fi_1}$ phase. This report confirms the prediction of Dolganov and Kats, i.e., in the ferrielectric 3-layer phases both quadratic and biquadratic interactions with nearest neighbors favor the increase in tilt angle.[30] Although for the compound $C_{12}F_3$, the $SmC^*_{Fi_1}$ phase coexists with the ferroelectric phase SmC^*, we can explain the absence of any particularity by the synclinic base structure of the SmC^* phase dominates.

4.4. Field-induced phase transition

The field-induced phenomena, such as the transitions under electric field, are of very great importance for display applications. We present and explain the experimental results of the field induced transitions through measuring the spontaneous polarization and threshold fields. Figures 7(a)–7(d) present the dependence of the polarization on bias voltages for different temperatures (i.e., different phases) for $C_{12}F_3$ compound.

The polarization plot corresponding to the SmC^*_α phase shows only one transition, under sufficient fields, to the unwound ferroelectric phase. This transition occurs directly, and only one threshold field appears.

For the SmC^* phase (81.6 °C) the curve also shows a typical dependence of polarization on voltage for a helical SmC^* phase. For low voltages, the polarization is found to gradually increase with voltage increasing and this corresponds to a distortion of the helix. The saturation is reached quickly.

However, fora temperature range of 67.2 °C–79.4 °C where we assume the coexistence of two polar phases ($SmC^* + SmC^*_{Fi_1}$), the macroscopic polarization possesses some interesting features. The dependence of the polarization on the voltage consists of three almost linear dependencies with different slopes (Fig. 7(c)).

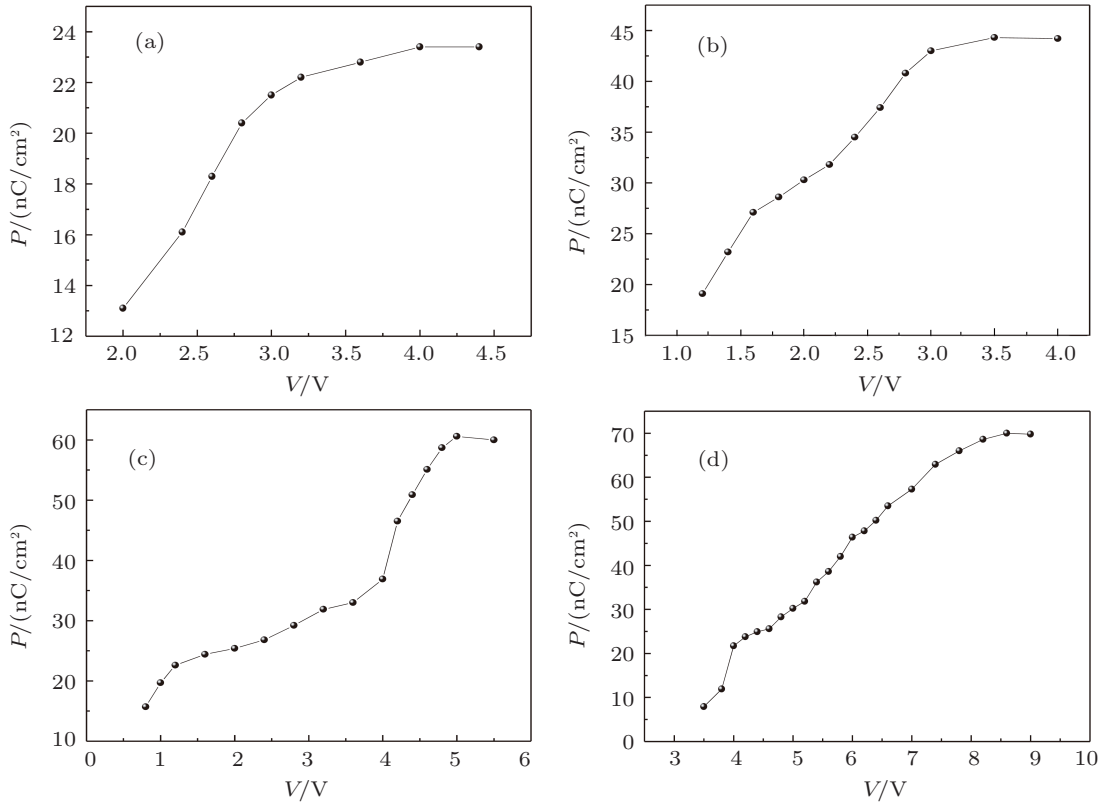


Fig. 7. (color online) Plots of the polarization versus bias voltages for (a) SmC^*_α, (b) SmC^*, (c) $SmC^* + SmC^*_{Fi_1}$, and (d) $SmC^*_{Fi_2}$ phases for $C_{12}F_3$ compound.

When SmC^* and $SmC^*_{Fi_1}$ phases coexist, the polarization varies slightly. The first transition from coexisting phases to intermediate phase is indiscernible due to the perturbation caused by the other polar phase and the weak threshold electric field inducing this transition.

We emphasize that in the SmC^* phase a polarization appears as soon as the input voltage is applied, which generates the unwinding of the helix. In the $SmC^*_{Fi_1}$ phase, we assist first a gradual distortion of the 3-layer arrangement. This distortion leads to the synclinic ferroelectric arrangement with the increase of the voltage. When the entire $SmC^*_{Fi_1}$ phase is transformed into SmC^*, the polarization grows gradually with voltage increasing as the helix is strongly being deformed with the increase of the electric field. At a higher voltage the polarization reaches a saturation value corresponding to the unwound SmC^* structure.

At 64.2 °C, the sample presents the $SmC^*_{Fi_2}$ phase at zero field, the polarization plot correspondingly shows typical ferrielectric dependence on voltage. For low voltages, polarization obeys almost linear dependence on voltage, corresponding to a distortion of the four-layer structure. Then at high voltages, the macroscopic polarization reaches a saturation value of the unwound SmC^* phase.

The constant current method allows the rapid localization of the transition threshold fields.[18,22] Figure 8 shows the evolution of the cell voltage with time under a constant current of 5 nA in the range of temperature of coexistence phases for the compound $C_{12}F_3$. Initially we observe a monotonic in-

crease due mainly to the charge of the capacitor, then one sees a plateau due to a first order transition.

The presence of two plateaus reveals the passage through an intermediate polar state between the phases null field, i.e., $SmC^*_{Fi_1}$ and SmC^*, and the unwound SmC^* phase.

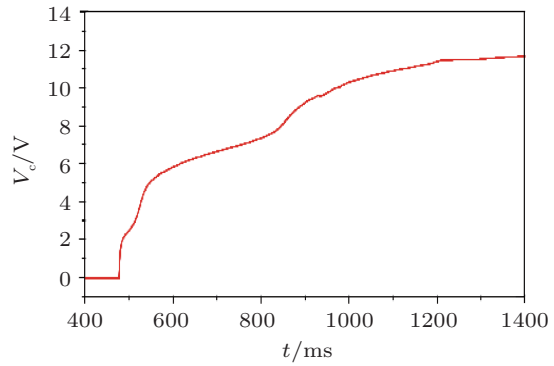


Fig. 8. (color online) Evolution of cell voltage with time under a constant current of 5 nA for $C_{12}F_3$.

4.5. (E,T) phase diagram

The field-temperature phase diagrams for both chiral smectic compounds studied are established. The method of plotting the (E,T) phase diagram through measuring the spontaneous polarization as a function of the electric field and the current constant method are used.

In the vicinity of the SmA^*–SmC^*_α phase transition, a pseudo transition temperature is clearly observed for both compounds.[31] Indeed, the electric field applied to the SmA^* phase ($P_s = 0$) induces an inclination and a polarization due to the electro–clinic effect. The new phase is denoted as SmC^*_{el}, dashed line between the SmA^* and $SmC^*_{unwound}$ phase domains in Figs. 9(a) and 9(b).

There are two different fields induced transitions in the 3-layer ferrielectric $SmC^*_{Fi_1}$ phase for both compounds. For the compound C_8F_2, two low threshold fields are detected. The 3-layer intermediate ferrielectric phase appears at first followed by the unwound SmC^* phase at sufficiently high fields. Note that the intermediate 3-layer structure is different from that of the $SmC^*_{Fi_1}$ phase described by the distorted clock model. The dynamics of this transition is very well described in Refs. [30], [31], and [21]. In the $C_{12}F_3$ compound, the ferrielectric $SmC^*_{Fi_1}$ phase coexists with the ferroelectric SmC^* one for a wide temperature range of 67.2 °C–79.4 °C while SmC^* phase only arises in the temperature interval of 79.4 °C–88 °C. We emphasize that the SmC^* phase directly transforms into the unwound phase SmC^* with a weak threshold value of the applied field. Whereas in the coexistence domain, the situation is more complicated, the compound transforms into the unwound SmC^* phase in the presence of the intermediate ferrielectric phase. The experimental determination of the field threshold in this interval is very difficult, which is because the transition line separating the coexistence domain from the intermediate phase is irregular.

In the C_8F_2 compound, the anticlinic SmC^*_A phase shows a typical behavior under electric field with a transition toward the intermediate ferrielectric phase at a sufficiently high value of the applied field. A similar behavior is observed in the $SmC^*_{Fi_2}$ phase in the compound $C12F3$ but with lower field values.

In conclusion, these diagrams show that no matter what the considered phase is, the transition to the unwound SmC^* phase is observed from a high value threshold field. This transition corresponds to a distortion of the helix where all the molecules have dipole moments oriented parallel to the applied field. Two situations are observed, i.e. the transition to the unwound phase SmC^* that takes place directly and the transition to the unwound phase SmC^* that happens through an intermediate ferroelectric polar phase.

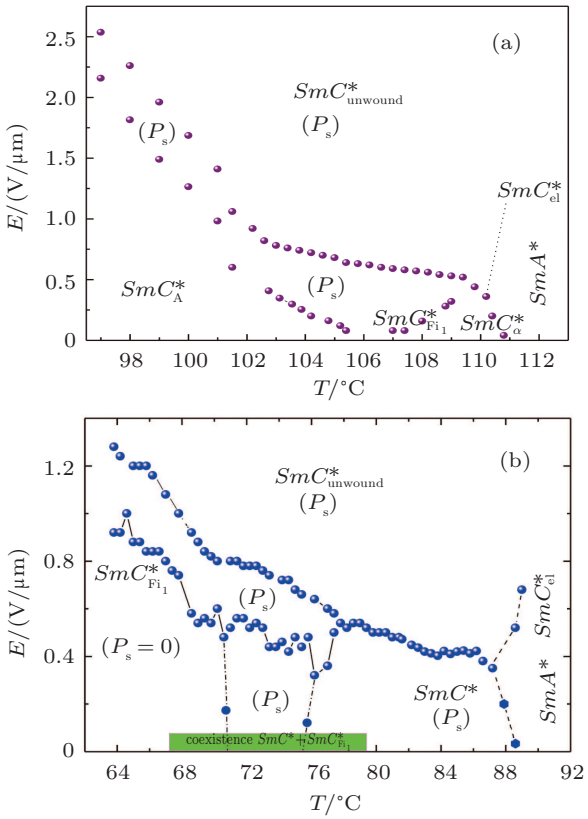


Fig. 9. (color online) Phase diagrams for (a) C_8F_2 and (b) $C_{12}F_3$ compounds.

5. Conclusions

Fluoro-substitution in liquid crystals is employed for many different reasons, but the overall aim is to modify material properties in order to optimize electro–optic properties in applications.[34,35]

In this paper, we have presented an experimental approach to studying the influences of the chemical structure and the fluorine position on the phase behavior of certain fluorinated chiral liquid crystals. We report the main results concerning the electro-optical properties and the (E,T) phase diagrams of two chiral smectic compounds "C_8F_2 and $C_{12}F_3$".

A comparison with the results obtained before on two other products of the same family, i.e., C_7F_2 and $C_{10}F_3$, is carried out.[18,20,25]

The comparison of the phase sequence and behavior under electric field of the compound "C_8F_2" with those of others fluorinated smectic liquid crystals highlights the effects of the chain length and the position of the fluorine atom on temperatures phase transition and the mesomorphic stability.

The results of optimized geometry study by using the molecular mechanics indicate that the physical properties of these compounds are strongly dependent on the location of the lateral fluoro-substituent.

Both the position of the fluorine atom and the length of the carbon chain affect the phase sequence of fluorinated chiral smectic liquid crystal. It appears that the position of the fluorine has an influence on the nature of the phases present. On the other hand, the length of the chains has an effect on the phase transition temperature.

References

[1] Demus D, Goodby J, Gray G W, Spiess H W and Vill V 1998 *Applications, Handbook of Liquid Crystals Vol. I — Fundamentals* (Weinheim: Wiley-Vch.) pp. 731–762

[2] Takatoh K, Hasegawa M, Koden M, Itoh N, Hasegawa R and Sakamoto M 2005 *Sakamoto Alignment Technologies and Applications of Liquid Crystal Devices* pp. 187–762

[3] Kriezis E E, Jones L A, Elston S J 2003 *Optical properties and applications of ferroelectric and antiferroelectric liquid crystals*

[4] Nguyen H T, Rouillon J C, Babeau A, Marcerou J P and Sigaud G 1999 *Liq. Cryst.* **26** 1007

[5] Essid S, Manai M, Gharbi A, Marcerou J P, Rouillon J C and Nguyen H T 2004 *Liq. Cryst.* **3** 1

[6] Hird M and Toyne K J 1998 *Mol. Cryst. Liq. Cryst.* **323** 1

[7] Hird M, Goodby J W, Lewis R A and Toyne K J 2003 *Mol. Cryst. Liq. Cryst.* **401** 115

[8] Hird M 2007 *Chem. Soc. Rev.* **36** 2070

[9] Dabrowski R, 2000 *Ferroelectrics* **243** 1

[10] Kromm P, Cortrait M and Nguyen H T 1996 *Liq. Cryst.* **21** 95

[11] Piecek W, Kula P, Raszewski Z, Perkowski P, Morawiak P, Kedzierski J, Dabrowski R and Sun X 2008 *Ferroelectrics* **365** 78

[12] Goswami D, Sinha D, Debnath A, Mandal P K, Gupta S K, Haase W, Ziobro D and Dabrowski R 2013 *J. Mol. Liq.* **182** 95

[13] Goswami D, Debnath A, Mandal P K, Węgłowska D, Dabrowski R and Czupryński K 2016 *Liq. Cryst.* **43** 1548

[14] Xiong J J, Shen D, Zheng Z G and Wang X Q 2016 *Chin. Phys.B* **25** 9

[15] Zheng Z, Ma J, Li W, Song J, Liu Y and Xuan L 2008 *Liq. Cryst.* **35** 885

[16] Hireoka K, Takanishi Y, Skarp K, Takezoe H and Fukuda A 1991 *Jap. J. Appl. Phys.* **30** L1819

[17] Isozaki T, Fujikawa T, Takezoe H, Fukuda A, Hagiwara T, Suzuki Y and Kawamura I 1993 *Phys. Rev. B* **48** 13439

[18] Marcerou J P, Nguyen H T, Bitri N, Gharbi A, Essid S and Soultani T 2007 *Eur. Phys. J. E* **23** 319

[19] Roy A and Madhusudana N V 1998 *Europhys. Lett.* **41** 501

[20] Essid S, Bitri N, Dhaouadi H, Gharbi A and Marcerou J P 2009 *Liq. Cryst.* **36** 359

[21] Gleeson H F, Jaradat S, Labeeb A and Osipov M 2012 *Ferroelectrics* **431** 40

[22] Dhaouadi M, Zgueb R, Riahi O, Trabelsi F and Othman T 2016 *Chin. Phys. B* **25** 057704

[23] de Gennes P G and Prost J 1993 *The Physic of Liquid Crystal*, 2nd edn. (Oxford: Clarendon Press)

[24] Garoff S and Meyer R B 1977 *Phys. Rev. Lett.* **38** 848

[25] Essid S, Manai, Gharbi A, Marcerou J P, Rouillon J C and Nguyen H T 2004 *Liq. Cryst.* **31** 1185

[26] Manai M 2006 "Etude des propriétés électriques et optiques de cristaux liquides présentant des phases smectiques chirales et les phases frustrées SmQ et L", Ph. D. Thesis (University of Tunisia and University of Bordeaux 1)

[27] Zgueb R, Dhaouadi H and Othman T 2014 *Liq. Cryst.* **41** 1394

[28] ChemDraw Ultra 8.0.3, CambridgeSoft

[29] Clark N A, Handschy M A and Lagerwall S T 1983 *Mol. Cryst. Liq. Crysr.* **94** 213

[30] Dolganov P V and Kats E I 2013 *Liq. Cryst. Rev.* **1** 127

[31] Trabelsi F, Dhaouadi H, Riahi O and Othman T 2018 *Chin. Phys. B* **27** 037701

[32] Jaradat S, Brimicombe P, Southern C, Siemianowski S, Pindak R, DiMasi E, Osipov and Gleeson H F 2008 *Phys. Rev. E* **77** 010701

[33] Jaradat S, Osipov M, PindakR and Gleeson H F 2011 *Appl. Phys. Lett.* **98** 043501

[34] Hird M 2011 *Liq. Cryst.* **38** 1467

[35] Thurmes W N, Wand M D, Vohra R T and More K M 1997 *SPIE* **3015** 0277-786X